Quantitative polarized light microscopy of unstained mammalian cochlear sections

Neil M. Kalwani[1,2]*, Cheng Ai Ong[1,2,3]*, Andrew C. Lysaght[1,2,4], Simon J. Haward[5,6], Gareth H. McKinley[5], Konstantina M. Stankovic[1,2,4]

*These authors contributed equally and are listed alphabetically.

[1]Department of Otology and Laryngology, Harvard Medical School, 25 Shattuck Street, Boston, MA 02115, USA
[2]Department of Otolaryngology, Massachusetts Eye and Ear Infirmary, 243 Charles St, Boston, MA 02114
[3]ENT Department, Hospital Queen Elizabeth, Karung Berkunci No. 2029, 88586 Kota Kinabalu, Sabah, Malaysia
[4]Program in Speech and Hearing Bioscience and Technology, Harvard / Massachusetts Institute of Technology Joint Division of Health Sciences and Technology, 77 Massachusetts Avenue, Cambridge, MA 02139, USA
[5]Department of Mechanical Engineering, Massachusetts Institute of Technology, 77 Massachusetts Avenue, Cambridge, MA 02139, USA
[6]Faculdade de Engenharia da Universidade do Porto, Centro de Estudos de Fenómenos de Transporte, Rua Dr. Roberto Frias, 4200-465 Porto, Portugal

Corresponding author:
Konstantina M. Stankovic
Department of Otolaryngology
Massachusetts Eye and Ear Infirmary
243 Charles St
Boston, MA 02114
Phone: 617-573-3972
Fax: 617-573-3914
Konstantina_Stankovich@meei.harvard.edu

Address of each author:
Neil M. Kalwani: Harvard Medical School, 25 Shattuck St, Boston MA 02115, EMAIL: neil_kalwani@hms.harvard.edu

Cheng Ai Ong: Jabatan ENT, Hospital Queen Elizabeth, Karung Berkunci No. 2029, 88586 Kota Kinabalu, Sabah, Malaysia. TEL: 6088-517555 ext 7650, FAX: 6088-318605, EMAIL: ongca181@hotmail.com

Andrew C. Lysaght: Massachusetts Eye and Ear Infirmary, 243 Charles St, Boston MA 02114. TEL: 617-573-6361, FAX: 617-473-3939, EMAIL: andrew_lysaght@meei.harvard.edu

Simon J. Haward: Faculdade de Engenharia da Universidade do Porto, Centro de Estudos de Fenómenos de Transporte, Rua Dr. Roberto Frias, 4200-465 Porto, Portugal. TEL: +351 225081404, FAX: +351 225081449, EMAIL: shaward@fe.up.pt

Gareth H. McKinley: Massachusetts Insitutute of Technology, Department of Mechanical Engineering, 77 Massachusetts Avenue, Cambridge MA 02139. TEL: 617-258-0754; FAX: 617-258-8559, EMAIL: gareth@mit.edu

Abstract

Hearing loss is the most common sensory deficit in the world, and it most frequently originates in the inner ear. Yet, the inner ear has been difficult to access for diagnosis because of its small size, delicate nature, complex 3D anatomy, and encasement in the densest bone in the body. Evolving optical methods are promising to afford cellular diagnosis of pathologic changes in the inner ear. To appropriately interpret results from these emerging technologies, it is important to characterize optical properties of cochlear tissues. Here we focus on that characterization using quantitative polarized light microscopy (qPLM) applied to unstained cochlear sections of the mouse, a common animal model of human hearing loss. We find that the most birefringent cochlear materials are collagen fibrils and myelin. Retardance of the otic capsule, the spiral ligament and the basilar membrane are substantially higher than that of other cochlear structures. Retardance of the spiral ligament and the basilar membrane decrease from the cochlear base to the apex, compared to the more uniform retardance of other structures. The intricate structural details revealed by qPLM of unstained cochlear sections *ex vivo* strongly motivate future application of polarization-sensitive optical coherence tomography to human cochlea *in vivo*.

Key words: quantitative polarized light microscopy, cochlea, birefringence, retardance, collagen, myelin

Introduction

Hearing loss is the most common sensory deficit in the world, affecting over 36 million Americans—18% of people 45-64 years of age, and ~50% of people over 75 years of age.[1] Yet the cause of deafness is not known for most affected individuals because the inner ear cannot be biopsied today without damaging residual hearing. Current clinical imaging modalities, including computed tomography (CT) and magnetic resonance imaging (MRI), are not sensitive enough to reveal cochlear microanatomy. Novel imaging modalities being developed for ultimate application in humans *in vivo* will require a full understanding of the optical properties of various cochlear structures.

One technique commonly used to investigate the optical properties of biological specimens is polarized light microscopy (PLM).[2] A conventional microscope can be converted into a simple polarization-sensitive microscope by placing perpendicularly oriented polarization filters into the beam of light before and after it passes the sample.[3] Without any intervening specimen, light passing the first filter is totally absorbed by the second filter. When biological samples are placed in the illumination path, however, certain structures change the polarization state of light that passes through them, allowing some component of that light to pass the second filter.[4]

In addition to sample-induced changes in polarization, some implementations of PLM are capable of detecting non-homogeneous alterations in wave propagation velocity. This phenomenon, often called sample retardance, occurs when the refractive index of the specimen is dependent on the polarization and direction of incoming light (a property known as birefringence). Materials that exhibit birefringence are anisotropic, or ordered in a directionally dependent way. This order can either be on the level of molecular bonds, resulting in intrinsic

birefringence, or on a submicroscopic level, resulting in form birefringence.[2] Two materials that are abundant in the cochlea, collagen and myelin, are known to exhibit birefringence.[2, 4] Importantly, defects of collagen and myelin in the cochlea have been implicated in disease; mutations in and autoimmunity against type II collagen[5-7] as well as demyelination of cochlear neurons[8, 9] all lead to hearing loss.

A unique advantage of PLM is that it allows for the structural characterization of biological specimens containing birefringent materials without having to stain or label them. PLM has been used in other fields to investigate collagen networks in tissues,[10] retinal nerve fiber layers,[11] meiotic spindles and microtubules within cells,[12, 13] and structural features that correlate with the health of ova to be used for intracytoplasmic sperm injection.[14] Despite its utility, PLM has only rarely been applied to the cochlea. Ren et al. used PLM to examine microcirculation in the guinea pig cochlea[15] whereas Wenzel et al. used PLM to examine collagen organization and content within the basilar membrane and other cochlear structures after laser irradiation.[16, 17]

One of the major drawbacks of standard PLM is that it is not a quantitative technique. The intensity of light observed when a birefringent material is viewed by a polarized light microscope depends on the angle of that material's optic axis relative to the transmission axes of the polarization filters.[4, 18] In a biological specimen, such as a histological section, birefringent materials may be oriented at different angles throughout the sample.

To address this limitation, a quantitative form of polarized light microscopy (qPLM) has been developed.[19, 20] In qPLM, two parameters related to the birefringent properties of the specimen are determined, independent of polarizer orientation, for each pixel in the acquired images:[19, 21] retardance (expressed in nanometers) and the average orientation of the polarization

axis with the greater index of refraction (the slow axis). qPLM has been used to examine collagen ultra-structure in normal and damaged articular cartilage,[21-23] collagen deposition in burn healing,[24] structural changes in myocardial tissue after infarction and regenerative treatments,[25] wall structural integrity of brain arteries,[26] and the paths of white matter tracts in the brain[27, 28] , among other applications. To the best of our knowledge, qPLM has never been applied to examine cochlear cross-sections.

In this study, we have applied qPLM to unstained murine cochlear cross-sections. We have focused on the mouse model because its cochlear anatomy and physiology is similar to that of humans, and many mouse models of human deafness are available to test the diagnostic power of this technique. To gain a basic understanding of the birefringent properties of the cochlea, we determined retardance values for various cochlear structures across two strains of mice commonly used in research.

Materials and methods

Experimental animals Six-week-old C57BL/6J (n=3) and CBA/CaJ (n=3) male mice (Jackson Laboratories) were used. All procedures were approved by the Massachusetts Eye & Ear Infirmary Animal Care and Use Committee.

Histological preparation Animals were anaesthetized with ketamine and xylazine. Transcardiac perfusion was performed using 4% paraformaldehyde. The oval and round windows were opened and intralabyrinthine perfusion was performed with the same fixative. Cochleae were isolated and placed in fixative for 2 hours, decalcified in EDTA for at least 3 days at room temperature, dehydrated, embedded in paraffin, and sectioned at a thickness of 10 μm. Section thickness was independently measured and confirmed to be 10 μm using a confocal microscope

(Leica TCS SP2 Spectral Confocal Laser Scanning Microscope). The main structures identifiable on an unstained cross section by differential interference contrast microscopy are labeled in Fig. 1.

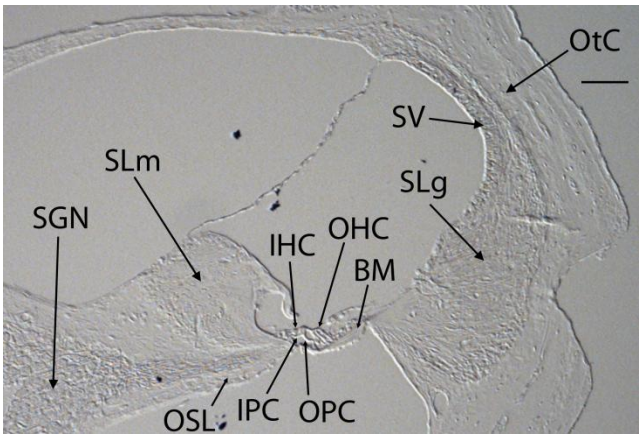

Fig. 1 Image of an unstained cross-section through the lower basal cochlear turn of a C57BL/6J mouse obtained using a differential interference contrast microscope. Key cochlear structures are labeled: SGN = spiral ganglion neuron cell bodies, SLm = spiral limbus, IHC = inner hair cell, OHC = outer hair cells, BM = basilar membrane, OSL = osseous spiral lamina, IPC= inner pillar cell, OPC = outer pillar cell, SLg = spiral ligament, SV = stria vascularis, OtC = otic capsule. The black bar represents 100 μm.

Quantitative polarized light microscopy Mid-modiolar sections were deparaffinized and coverslipped (unstained) with Permount mounting medium (Fisher Scientific). Slides were imaged using the Abrio Birefringence Imaging System (Cambridge Research & Instrumentation Inc.), which has been described in detail previously.[29] Briefly, specimens are placed on the stage of an inverted microscope (Nikon Eclipse TE 2000-S). Circularly polarized monochromatic light (wavelength 546 nm) passes through the sample and then through a universal compensator made from two computer-controlled liquid crystal (LC) variable retarder plates. Images of the specimen are acquired at five different settings of the LC retarder plates by a charge-coupled device (CCD) imaging sensor, and are transferred to a computer. Polarimetric algorithms[29] are used to convert the data from these images into a single full-field map of retardance values and

slow axis orientations. The system can determine retardance values to a nominal resolution of 0.02 nm. Retardance measurements of cochlear structures were made by finding average pixel intensities in grayscale retardance magnitude images using ImageJ (U.S. National Institutes of Health). Results are expressed as means +/- standard error of the mean.

Retardance is generated between the orthogonally polarized components of light transmitted through a birefringent material as a result of the difference in their propagation velocities.[30] The retardance (Γ) divided by the path length of the light through the material (d) is equal to the birefringence (Δn): $\Delta n = \Gamma / d$. The path length is difficult to determine, especially in tissue because it is highly scattering. The retardance, however, is proportional to sample birefringence if the path length is held constant. Because our section thickness was the same across measurements, we use "retardance" and "birefringence" interchangeably. Retardance measurements are independent of the wavelength of light transmitted through the sample. Retardance values can be converted to phase shifts (Φ), measured in radians, which are dependent on wavelength (λ) as follows: $\Phi = 2\pi * \Gamma / \lambda$.

Immunohistochemistry Deparaffinized sections for collagen immunolabeling were incubated in pepsin solution (Thermo Scientific, AP-9007-005) for 10 minutes at 37°C in a humidified chamber. All sections were washed in 0.01M PBS, pH 7.4, exposed to blocking serum (5% normal horse serum (NHS) + Triton X) for 1 hour at room temperature in a humidified chamber, incubated with 1:100 mouse anti-mouse collagen type 2 antibody (Thermo Scientific, Collagen II Ab-2 Clone 2B1.5, MS-235-P0) or 1:1000 chicken anti-mouse myelin basic protein (MBP) antibody (Novus Biologicals, NB100-1603) overnight in a humidified chamber, rinsed in PBS and covered with 1:1000 Alexa Fluor 568 rabbit anti-mouse antibody (Invitrogen, A10037) (collagen) or 1:1000 Alexa Fluor 488 goat anti-chicken antibody (Invitrogen, A11039) (MBP) in

1% NHS for 1 hour at room temperature in a humidified chamber. Sections were coverslipped with Vectashield mounting medium (Vector Laboratories, H-1000) and imaged using a fluorescence microscope (Nikon Eclipse E800).

Results and Discussion

Pseudocolor retardance magnitude and orientation images of unstained cochlear cross sections through the lower basal turn reveal intricate networks of fibers running throughout the cochlea [Fig. 2]. These networks were more elaborate than could be appreciated with differential interference contrast microscopy [Fig. 1]. Fibers observed by qPLM converged on the basilar membrane from the spiral limbus and from within the osseous spiral lamina (OSL), and spread from the basilar membrane into the spiral ligament. The same pattern was observed in the lower apical turn [Fig. 3], although the retardance magnitudes appeared to be lower.

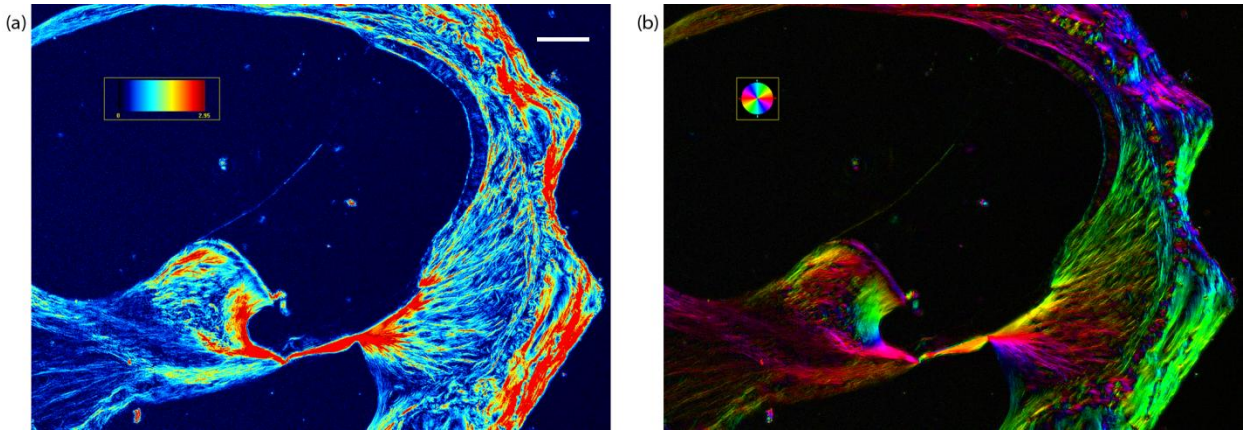

Fig. 2 (A) Pseudocolor retardance magnitude and (B) orientation images of a cross-section through the lower basal cochlear turn of a C57BL/6J mouse. The colored bar in (A) indicates the scale for retardance magnitude from 0 to 2.95 nm, and the white bar represents 100 μm. The colored circle in (B) indicates the correspondence between pixel color and orientation of the slow axis.

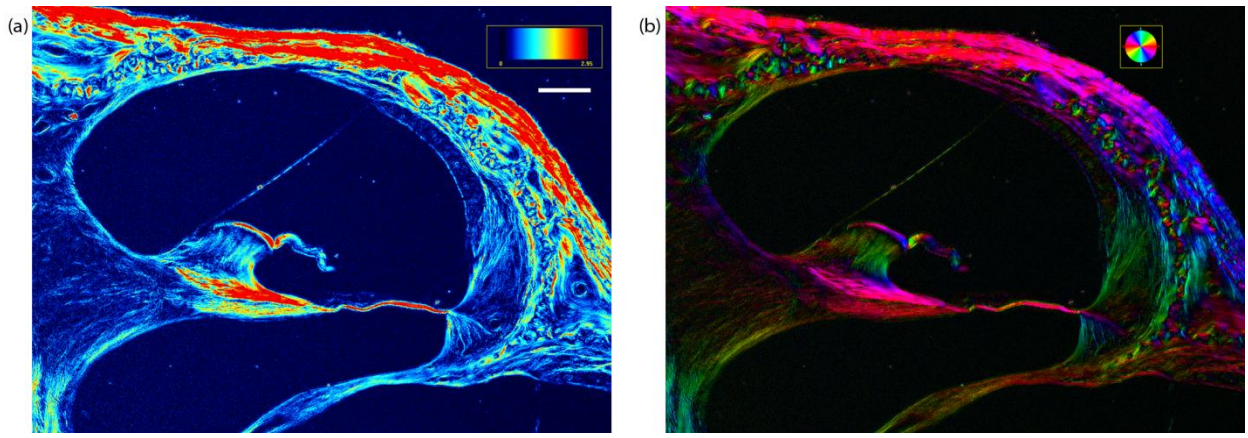

Fig. 3 (A) Pseudocolor retardance magnitude and (B) orientation images of a cross-section through the lower apical cochlear turn of a C57BL/6J mouse. The colored bar in (A) indicates the scale for retardance magnitude from 0 to 2.95 nm, and the white bar represents 100 μm. The colored circle in (B) indicates the correspondence between pixel color and orientation of the slow axis.

To determine the sources of the observed fiber networks, we used immunohistochemistry directed against collagen and myelin, which are known to exhibit birefringence. We focused on type II collagen [Fig. 4(a)] because it is the main fibrillar component of the mammalian cochlea,[31-34] and on myelin basic protein [Fig. 4(b)] because it is a main component of peripheral myelin that ensheathes the processes of cochlear neurons within the osseous spiral lamina.[35] Immunoreactivity for type II collagen revealed a strong signal in the spiral limbus, basilar membrane, spiral ligament, and otic capsule [Fig. 4(a)], consistent with previous reports of a radially oriented network of type II collagen fibrils, identified by immunostaining and electron microscopy, beginning in the spiral limbus, converging on the insertion of the basilar membrane, and spreading into the spiral ligament toward the stria vascularis.[31, 33] Immunoreactivity for myelin basic protein was localized to the myelinated nerve fibers within the osseous spiral lamina [Fig. 4(b)]. This pattern was complementary to the strong collagen II immunoreactivity of the osseous spiral lamina [Fig. 4(a)]. Neither type II collagen nor myelin basic protein were observed within the stria vascularis, which exhibited a weak retardance signal.

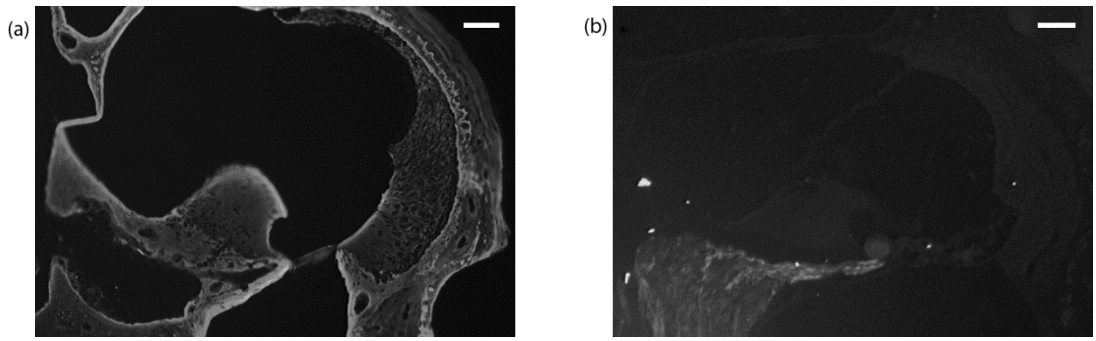

Fig. 4 Cross-sections through a basal cochlear turn of a CBA/CaJ mouse with immunofluorescence labeling for (A) type II collagen and (B) myelin basic protein imaged with a fluorescence microscope. The white bars in (A) and (B) represent 100 μm.

Collagen is known to exhibit both intrinsic and form birefringence. The intensity of birefringence of a collagen network thus depends both on the collagen density and on the extent of collagen organization at the fibrillar level.[2] The optic axis of a collagen network is oriented along the length of the fibrils and is the slow axis (positive birefringence).[36, 37] The optic axis of myelin is oriented along the length of the axons, but it is the fast axis (negative birefringence). In sections that have had lipids extracted, such as paraffin sections, however, myelin exhibits positive birefringence.[4]

If the fiber networks evident in the qPLM images do represent type II collagen fibrils and myelinated neuronal processes, it is significant that the level of fiber detail in the qPLM images is much greater than that observed in immunofluorescence images. qPLM may thus provide a superior means of qualitatively evaluating the organization of collagen fibrils and neuronal processes in cochlear sections, while saving the tissue, time, and expense required to perform immunohistochemistry.

One of the primary strengths of the qPLM technique is its ability to provide objective, quantitative information on tissue organization. To explore the utility of these data, we determined mean retardance values (n=3) for a variety of cochlear structures at each cochlear

turn [Fig. 5 and 6]. The retardance values for C57BL/6J and CBA/CaJ mice were similar for all structures. This is important because each strain offers specific experimental advantages. Many models of hearing loss have been developed in the C57BL/6J strain, which exhibits early, age-related hearing loss at high frequencies, whereas the CBA/CaJ strain has good hearing across frequencies into old age. The similarity in cochlear retardance in C57BL/6J and CBA/CaJ mice is likely due to the young age of the imaged mice as both strains have equally good hearing at 6 weeks of age.

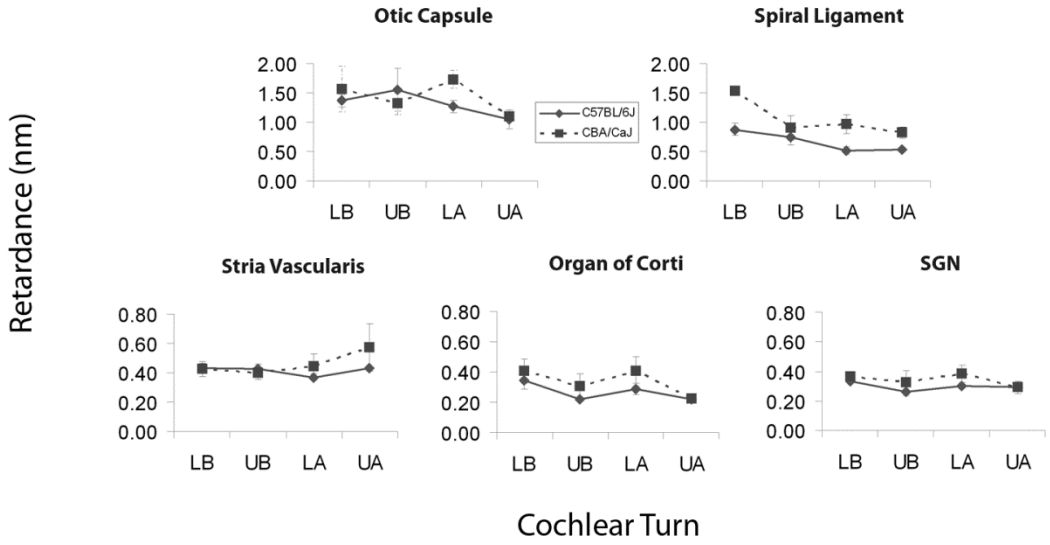

Fig. 5 Mean retardance values with error bars (in nm) of various cochlear structures plotted for each cochlear turn in C57BL/6J (n = 3) and CBA/CaJ mice (n = 3). LB = lower basal turn, UB = upper basal turn, LA = lower apical turn, and UA = upper apical turn. SGN = spiral ganglion neuron cell bodies. Error bars depict standard errors of the mean.

For a given turn, different cochlear structures exhibited different levels of birefringence, with the basilar membrane, spiral ligament and otic capsule being most birefringent. For example, when focusing on the lower basal turn, the mean retardance of the basilar membrane under the outer hair cells was 5.03 ± 0.47 nm in the C57BL/6J mice and 5.07 ± 0.26 nm in the CBA/CaJ mice, which was about 5 times higher than the mean retardance of the spiral ligament

(0.88 ± 0.11 nm in the C57BL/6J mice and 1.54 ± 0.07 nm in the CBA/CaJ mice), and about 12 times higher than the mean retardance of the stria vascularis (0.43 ± 0.03 nm in the C57BL/6J mice and 0.43 ± 0.05 nm in the CBA/CaJ mice). Some cochlear structures, such as the basilar membrane and the spiral ligament, demonstrated a decreasing gradient of birefringence from the cochlear base to the apex whereas other structures had more uniform retardance across the cochlear length. For example, the mean retardance of the basilar membrane under the outer hair cells at the upper apical turn was 0.79 ± 0.14 nm in the C57BL/6J mice and 0.99 ± 0.17 nm in the CBA/CaJ mice, which was about 5-6 times smaller, and significantly different from the values at the lower basal turn ($p = 0.00096$ and 0.00020 respectively). Likewise, the mean retardance of the spiral ligament at the upper apical turn was 0.53 ± 0.03 nm in the C57BL/6J mice and 0.83 ± 0.10 nm in the CBA/CaJ mice, both of which were significantly smaller than the values at the lower basal turn ($p = 0.0036$ and 0.0043 respectively).

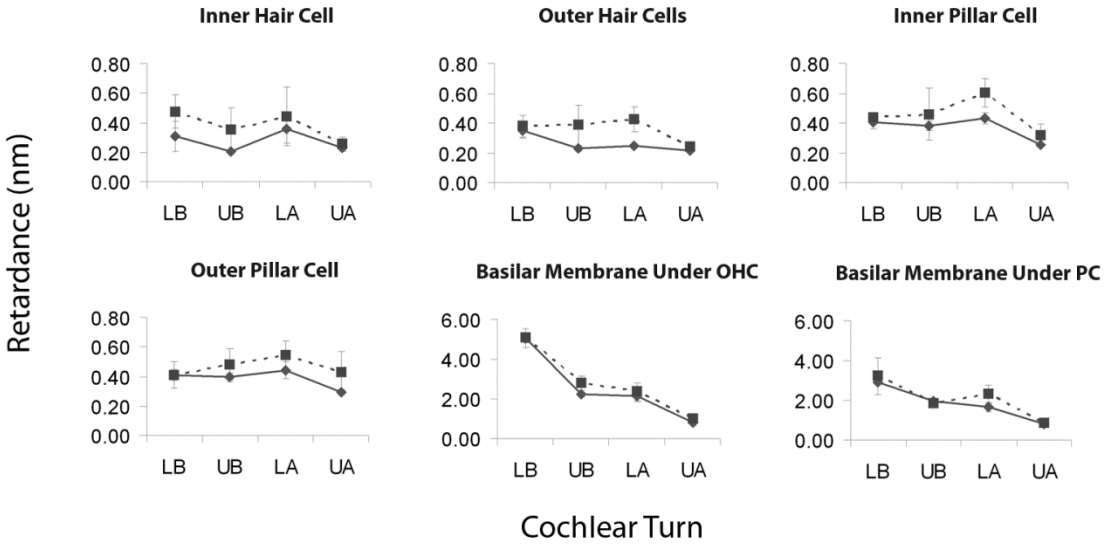

Fig. 6 Mean retardance values with error bars (in nm) of various cochlear structures plotted for each cochlear turn in C57BL/6J (n = 3) and CBA/CaJ mice (n = 3). OHC = outer hair cells, PC = pillar cells. Error bars depict standard errors of the mean.

We have shown that qPLM provides a powerful tool for qualitative and quantitative analysis of the submicroscopic organization of various cochlear structures. Our results motivate future application of qPLM to characterize various murine models of human hearing loss, based on specific changes in the birefringent properties of cochlear structures. In light of our recent study demonstrating that the optical properties of fixed cochlear tissues are similar to those of unfixed specimens[38], qPLM data from the fixed specimens may ultimately be adopted as new noninvasive imaging modalities in humans *in vivo* to guide diagnosis and management.

One such imaging modality is optical coherence tomography (OCT), a noninvasive technique that generates cross-sectional images of tissue based on backscattered light from a focused beam directed at the sample. The technique is similar to ultrasound, but uses light instead of sound, allowing for the acquisition of images with high spatial resolution. The OCT resolution, between 2 and 20 μm, exceeds that provided by CT and MRI and is sufficient to allow visualization of cochlear structures.[39] In fact, OCT has recently been used to image murine cochlear microanatomy, including the basilar membrane, spiral ligament, and organ of Corti.[40-44]

An enhanced version of OCT, polarization-sensitive OCT (PS-OCT), allows for measurement of sample birefringence[45] and the orientation of the fast axis.[46-48] This technique has already been successfully applied to qualitatively and quantitatively examine collagen birefringence patterns in tissue, including human skin.[49] However, PS-OCT has not been applied to the cochlea. Assuming linear path lengths, we found the birefringence of cochlear structures to vary between 2.0×10^{-5} and 5.1×10^{-4}. PS-OCT may be sufficiently sensitive to detect subtle changes in cochlear birefringence because PS-OCT has been used to determine tissue birefringence levels as low as 2.8×10^{-6} [50]. Our results strongly motivate future

application of imaging modalities such as PS-OCT to the human inner ear *in vivo* to obtain a fundamental new insight into the workings of the inner ear, to establish microstructural diagnosis, and to guide therapy. Successful application of these imaging modalities to the cochlea will require a complete understanding of the baseline optical properties of cochlear structures, including birefringence, and how these properties are altered in disease states.

Conclusion

We report the first characterization of optical properties of unstained cochlear structures using qPLM applied to histologic sections. Our results suggest that qPLM has important advantages over immunohistochemistry when qualitatively evaluating the organization of collagen fibrils and myelinated neuronal processes because qPLM provides intricately detailed information on unstained fiber networks, thus saving the tissue, time, and expense required to perform immunohistochemistry. Our results strongly motivate future application of PS-OCT and similar imaging technologies to the human inner ear *in vivo*.

Acknowledgments

We are grateful for the support of the National Institute on Deafness and other Communication Disorders grants K08 DC010419 (K.M.S.) and T32 DC00038 (A.C.L.), the Bertarelli Foundation (K.M.S.), the Harvard Medical School Scholars in Medicine Office (N.M.K.) and the Malaysian Federal Training Scholarship (C.A.O.). S.J.H. and G.H.M. gratefully acknowledge financial support from NASA Microgravity Fluid Sciences (Code UG) grant NNX09AV99G. We thank Drs. Deborah Perez Fernandez and Johannes Soulages for preliminary studies.

References

1. "Quick Statistics," *National Institute on Deafness and Other Communication Disorders,* 16 June 2010, (accessed 14 November 2012).

2. H. Bennett, "Methods Applicable to the Study of both Fresh and Fixed Materials with Polarized Light," in *McClung's Handbook of Microscopical Technique,* R. M. Jones, Ed., pp. 591-677, Paul B. Hoeber, New York, NY (1950).

3. F. Massoumian, R. Juskaitis, M. A. Neil, and T. Wilson, "Quantitative polarized light microscopy," *J. Microsc.* **209**(Pt 1), 13-22 (2003).

4. M. Wolman, "Polarized light microscopy as a tool of diagnostic pathology," *J. Histochem. Cytochem.* **23**(1), 21-50 (1975).

5. P. H. Byers, "Inherited disorders of collagen gene structure and expression," *Am. J. Med. Genet.* **34**(1), 72-80 (1989).

6. H. Kuivaniemi, G. Tromp, and D. J. Prockop, "Mutations in collagen genes: causes of rare and some common diseases in humans," *FASEB J.* **5**(7), 2052-2060 (1991).

7. T. Joliat, J. Seyer, J. Bernstein, M. Krug, X. J. Ye, J. S. Cho, T. Fujiyoshi, and T. J. Yoo, "Antibodies against a 30 kilodalton cochlear protein and type II and IX collagens in the serum of patients with inner ear diseases," *Ann. Otol. Rhinol. Laryngol.* **101**(12), 1000-1006 (1992).

8. H. Spoendlin, "Factors inducing retrograde degeneration of the cochlear nerve," *Ann. Otol. Rhinol. Laryngol. Suppl.* **112**, 76-82 (1984).

9. P. A. Leake and G. T. Hradek, "Cochlear pathology of long term neomycin induced deafness in cats," *Hear. Res.* **33**(1), 11-33 (1988).

10. K. Fackler, L. Klein, and A. Hiltner, "Polarizing light microscopy of intestine and its relationship to mechanical behaviour," *J. Microsc.* **124**(Pt 3), 305-311 (1981).

11. X. R. Huang, H. Bagga, D. S. Greenfield, and R. W. Knighton, "Variation of peripapillary retinal nerve fiber layer birefringence in normal human subjects," *Invest. Ophthalmol. Vis. Sci.* **45**(9), 3073-3080 (2004).

12. L. Liu, J. R. Trimarchi, R. Oldenbourg, and D. L. Keefe, "Increased birefringence in the meiotic spindle provides a new marker for the onset of activation in living oocytes," *Biol. Reprod.* **63**(1), 251-258 (2000).

13. P. Tran, E. D. Salmon, and R. Oldenbourg, "Quantifying single and bundled microtubules with the polarized light microscope," *Biol. Bull.* **189**(2), 206 (1995).

14. Y. Shen, T. Stalf, C. Mehnert, U. Eichenlaub-Ritter, and H. R. Tinneberg, "High magnitude of light retardation by the zona pellucida is associated with conception cycles," *Hum. Reprod.* **20**(6), 1596-1606 (2005).

15. T. Ren, X. Lin, and A. L. Nuttall, "Polarized-light intravital microscopy for study of cochlear microcirculation," *Microvasc. Res.* **46**(3), 383-393 (1993).

16. G. I. Wenzel, B. Pikkula, C. H. Choi, B. Anvari, and J. S. Oghalai, "Laser irradiation of the guinea pig basilar membrane," *Lasers Surg. Med.* **35**(3), 174-180 (2004).

17. G. I. Wenzel, B. Anvari, A. Mazhar, B. Pikkula, and J. S. Oghalai, "Laser-induced collagen remodeling and deposition within the basilar membrane of the mouse cochlea," *J. Biomed. Opt.* **12**(2), 021007 (2007).

18. P. S. Jouk, Y. Usson, G. Michalowicz, and F. Parazza, "Mapping of the orientation of myocardial cells by means of polarized light and confocal scanning laser microscopy," *Microsc. Res. Tech.* **30**(6), 480-490 (1995).

19. R. Oldenbourg and G. Mei, "New polarized light microscope with precision universal compensator," *J. Microsc.* **180**(Pt 2), 140-147 (1995).

20. R. Oldenbourg, "A new view on polarization microscopy," *Nature* **381**(6585), 811-812 (1996).

21. J. Rieppo, J. Hallikainen, J. S. Jurvelin, I. Kiviranta, H. J. Helminen, and M. M. Hyttinen, "Practical considerations in the use of polarized light microscopy in the analysis of the collagen network in articular cartilage," *Microsc. Res. Tech.* **71**(4), 279-287 (2008).

22. J. P. Arokoski, M. M. Hyttinen, T. Lapvetelainen, P. Takacs, B. Kosztaczky, L. Modis, V. Kovanen, and H. Helminen, "Decreased birefringence of the superficial zone collagen network in the canine knee (stifle) articular cartilage after long distance running training, detected by quantitative polarised light microscopy," *Ann. Rheum. Dis.* **55**(4), 253-264 (1996).

23. Y. Xia, J. B. Moody, N. Burton-Wurster, and G. Lust, "Quantitative in situ correlation between microscopic MRI and polarized light microscopy studies of articular cartilage," *Osteoarthritis Cartilage* **9**(5), 393-406 (2001).

24. S. V. Madibally, V. Solomon, R. N. Mitchell, L. Van De Water, M. L. Yarmush, and M. Toner, "Influence of insulin therapy on burn wound healing in rats," *J. Surg. Res.* **109**(2), 92-100 (2003).

25. M. F. Wood, N. Ghosh, M. A. Wallenburg, S. H. Li, R. D. Weisel, B. C. Wilson, R. K. Li, and I. A. Vitkin, "Polarization birefringence measurements for characterizing the myocardium, including healthy, infarcted, and stem-cell-regenerated tissues," *J. Biomed. Opt.* **15**(4), 047009 (2010).

26. A. J. Rowe, H. M. Finlay, and P. B. Canham, "Collagen biomechanics in cerebral arteries and bifurcations assessed by polarizing microscopy," *J. Vasc. Res.* **40**(4), 406-415 (2003).

27. H. Axer, M. Axer, T. Krings, and D. G. Keyserlingk, "Quantitative estimation of 3-D fiber course in gross histological sections of the human brain using polarized light," *J. Neurosci. Methods* **105**(2), 121-131 (2001).

28. L. Larsen, L. D. Griffin, D. Grassel, O. W. Witte, and H. Axer, "Polarized light imaging of white matter architecture," *Microsc. Res. Tech.* **70**(10), 851-863 (2007).

29. M. Shribak and R. Oldenbourg, "Techniques for fast and sensitive measurements of two-dimensional birefringence distributions," *Appl. Opt.* **42**(16), 3009-3017 (2003).

30. W. A. Shurcliff, *Polarized Light, Production and Use,* Harvard University Press, Cambridge, Massachusetts (1962).

31. N. B. Slepecky, J. E. Savage, and T. J. Yoo, "Localization of type II, IX and V collagen in the inner ear," *Acta Otolaryngol.* **112**(4), 611-617 (1992).

32. H. Kaname, T. Yoshihara, T. Ishii, H. Tatsuoka, and T. Chiba, "Ultrastructural and immunocytochemical study of the subepithelial fiber component of the guinea pig inner ear," *J. Electron. Microsc. (Tokyo)* **43**(6), 394-397 (1994).

33. V. Tsuprun and P. Santi, "Ultrastructure and immunohistochemical identification of the extracellular matrix of the chinchilla cochlea," *Hear. Res.* **129**(1-2), 35-49 (1999).

34. F. J. Dreiling, M. M. Henson, and O. W. Henson Jr, "The presence and arrangement of type II collagen in the basilar membrane," *Hear. Res.* **166**(1-2), 166-180 (2002).

35. P. A. Hurley, J. M. Crook, and R. K. Shepherd, "Schwann cells revert to non-myelinating phenotypes in the deafened rat cochlea," *Eur. J. Neurosci.* **26**(7), 1813-1821 (2007).

36. D. B. Brewer, "Differences in the fine structure of collagen and reticulin as revealed by the polarising microscope," *Journal of Pathology & Bacteriology* **74**, 371-385 (1957).

37. D. M. Maurice, "The Cornea and Sclera," in *The Eye, Vol I,* H. Davson, Ed., pp. 289-368, Academic Press, New York (1962).

38. X. Yang, Y. Pu, C. L. Hsieh, C. A. Ong, D. Psaltis, and K. M. Stankovic, "Two-photon microscopy of the mouse cochlea in situ for cellular diagnosis," *J. Biomed. Opt.* **18**(3), 31104 (2013).

39. D. Huang, E. A. Swanson, C. P. Lin, J. S. Schuman, W. G. Stinson, W. Chang, M. R. Hee, T. Flotte, K. Gregory, and C. A. Puliafito, "Optical coherence tomography," *Science* **254**(5035), 1178-1181 (1991).

40. B. J. Wong, J. F. de Boer, B. H. Park, Z. Chen, and J. S. Nelson, "Optical coherence tomography of the rat cochlea," *J. Biomed. Opt.* **5**(4), 367-370 (2000).

41. B. J. Wong, Y. Zhao, M. Yamaguchi, N. Nassif, Z. Chen, and J. F. De Boer, "Imaging the internal structure of the rat cochlea using optical coherence tomography at 0.827 microm and 1.3 microm," *Otolaryngol. Head. Neck. Surg.* **130**(3), 334-338 (2004).

42. A. Sepehr, H. R. Djalilian, J. E. Chang, Z. Chen, and B. J. Wong, "Optical coherence tomography of the cochlea in the porcine model," *Laryngoscope* **118**(8), 1449-1451 (2008).

43. J. Lin, H. Staecker, and M. S. Jafri, "Optical coherence tomography imaging of the inner ear: a feasibility study with implications for cochlear implantation," *Ann. Otol. Rhinol. Laryngol.* **117**(5), 341-346 (2008).

44. H. M. Subhash, V. Davila, H. Sun, A. T. Nguyen-Huynh, A. L. Nuttall, and R. K. Wang, "Volumetric in vivo imaging of intracochlear microstructures in mice by high-speed spectral domain optical coherence tomography," *J. Biomed. Opt.* **15**(3), 036024 (2010).

45. J. F. de Boer, T. E. Milner, M. J. van Gemert, and J. S. Nelson, "Two-dimensional birefringence imaging in biological tissue by polarization-sensitive optical coherence tomography," *Opt. Lett.* **22**(12), 934-936 (1997).

46. J. F. de Boer, T. E. Milner, and J. S. Nelson, "Determination of the depth-resolved Stokes parameters of light backscattered from turbid media by use of polarization-sensitive optical coherence tomography," *Opt. Lett.* **24**(5), 300-302 (1999).

47. J. E. Roth, J. A. Kozak, S. Yazdanfar, A. M. Rollins, and J. A. Izatt, "Simplified method for polarization-sensitive optical coherence tomography," *Opt. Lett.* **26**(14), 1069-1071 (2001).

48. C. Hitzenberger, E. Goetzinger, M. Sticker, M. Pircher, and A. Fercher, "Measurement and imaging of birefringence and optic axis orientation by phase resolved polarization sensitive optical coherence tomography," *Opt. Express* **9**(13), 780-790 (2001).

49. M. C. Pierce, R. L. Sheridan, B. Hyle Park, B. Cense, and J. F. de Boer, "Collagen denaturation can be quantified in burned human skin using polarization-sensitive optical coherence tomography," *Burns* **30**(6), 511-517 (2004).

50. C. C. Wu, Y. M. Wang, L. S. Lu, C. W. Sun, C. W. Lu, M. T. Tsai, and C. C. Yang, "Tissue birefringence of hypercholesterolemic rat liver measured with polarization-sensitive optical coherence tomography," *J. Biomed. Opt.* **12**(6), 064022 (2007).

Fig. 1 Image of an unstained cross-section through the lower basal cochlear turn of a C57BL/6J mouse obtained using a differential interference contrast microscope. Key cochlear structures are labeled: SGN = spiral ganglion neuron cell bodies, SLm = spiral limbus, IHC = inner hair cell, OHC = outer hair cells, BM = basilar membrane, OSL = osseous spiral lamina, IPC= inner pillar cell, OPC = outer pillar cell, SLg = spiral ligament, SV = stria vascularis, OtC = otic capsule. The black bar represents 100 μm.

Fig. 2 (A) Pseudocolor retardance magnitude and (B) orientation images of a cross-section through the lower basal cochlear turn of a C57BL/6J mouse. The colored bar in (A) indicates the scale for retardance magnitude from 0 to 2.95 nm, and the white bar represents 100 μm. The colored circle in (B) indicates the correspondence between pixel color and orientation of the slow axis.

Fig. 3 (A) Pseudocolor retardance magnitude and (B) orientation images of a cross-section through the lower apical cochlear turn of a C57BL/6J mouse. The colored bar in (A) indicates the scale for retardance magnitude from 0 to 2.95 nm, and the white bar represents 100 μm. The colored circle in (B) indicates the correspondence between pixel color and orientation of the slow axis.

Fig. 4 Cross-sections through the (A) lower basal and (B) upper basal cochlear turns of a CBA/CaJ mouse with immunofluorescence labeling for (A) type II collagen and (B) myelin basic protein imaged with a fluorescence microscope. The white bars in (A) and (B) represent 100 μm.

Fig. 5 Mean retardance values with error bars (in nm) of various cochlear structures plotted for each cochlear turn in C57BL/6J (n = 3) and CBA/CaJ mice (n = 3). LB = lower basal turn, UB = upper basal turn, LA = lower apical turn, and UA = upper apical turn. SGN = spiral ganglion neuron cell bodies. Error bars depict standard errors of the mean.

Fig. 6 Mean retardance values with error bars (in nm) of various cochlear structures plotted for each cochlear turn in C57BL/6J (n = 3) and CBA/CaJ mice (n = 3). OHC = outer hair cells, PC = pillar cells. Error bars depict standard errors of the mean.